ELSEVIER

Chemical Physics 230 (1998) 1–11

Chemical Physics

Theoretical analysis of reactions related to the HNO_2 energy surface: OH + NO and H + NO_2

Minh Tho Nguyen [1], Raman Sumathi [2], Debasis Sengupta, Jozef Peeters

Department of Chemistry, University of Leuven, Celestijnenlaan 200F, B-3001 Leuven, Belgium

Received 3 September 1997

Abstract

The reactions occurring on the lowest singlet potential energy surface (PES) of the HNO_2 system, including the H + NO_2 and OH + NO entry channels, have been studied using ab initio molecular orbital (MO) and density functional (DFT) theories. The energetic and molecular parameters derived from coupled cluster singles and doubles with triples correction (CCSD(T)) and the B3LYP-DFT calculations using the 6-311 + + G(3df,2p) basis set, based on their respective optimised geometries obtained respectively, with a 6-31G(d,p) and 6-311 + + G(d,p) basis sets, have then been utilized to compute the rate constants of the different competitive channels in the HNO_2 system within the framework of a quantum version of Rice-Ramsperger-Kassel theory (QRRK) and a canonical variational transition state theory (CVTST). Various thermochemical parameters of the [HNO_2] species have also been computed. © 1998 Elsevier Science B.V.

1. Introduction

The lowest singlet potential energy surface of the HNO_2 system is important due to the presence of few reaction channels which play a major role in atmospheric and combustion chemistry. The important reactions, in particular, are

$$NH(^3\Sigma^-) + O_2(^3\Sigma_g^-) \rightarrow OH(^2\Pi) + NO(^2\Pi),$$

$$HNO + O \text{ and/or } NO_2 + H \quad (a)$$

$$H + NO_2(^2A_1) \rightarrow OH(^2\Pi) + NO(^2\Pi) \quad (b)$$

$$HONO(^1A') \rightarrow OH(^2\Pi) + NO(^2\Pi) \quad (c)$$

While the reaction (a) occurs in the ammonia + oxygen flame [1], the very fast reaction (b) and its reverse are believed to involve in the oxidation of NO, which converts NO to NO_2 [2]. The kinetics of both reactions (a) and (b) have been investigated in a number of previous experimental studies [1,3–9]. Most of the available high temperature rate constants for reaction (a) have been inferred from applications of kinetic models to flame [10–13]. A recent review by Dean et al. [14] on NH + O_2 system compiles the complete literature. Both reactions (a) and (b) have been shown to yield OH + NO as their final product. These radicals are also the products of photodissociation of nitrous acid (reaction c) [15]. The suggested rate constant values [16] $k_0(N_2)$ and k_∞ for the reverse reaction (−c), OH + NO + M → HONO + M are 7.4×10^{-31} cm^6 molecule^{-2} s^{-1} and 3.2×10^{-11} cm^3 molecule^{-1} s^{-1}. Surprisingly, the kinetics of the reverse reactions (−a) and (−b) between NO and OH radicals have, to our

[1] E-mail: minh.nguyen@chem.kuleuven.ac.be.

[2] On leave from Manonmanium Sundaranar Univeristy, Tirunelveli-627 002, India.

PII S0301-0104(97)00383-2

knowledge, never been reported even though these reactants are simultaneously present in flames, for example, H_2–O_2–NO system.

The HNO_2 potential energy surface (PES) comprising reactions (a) and (b) has been studied by Fueno and coworkers [17,18] using a multireference configuration interaction method (MCSCF/MRDCI). They have evaluated the rate constant of the reaction (a) via the following reaction scheme

$$NH(^3\Sigma^-) + O_2(^3\Sigma_g^-) \rightarrow [HNOO]^* \rightarrow NO + OH$$

However, no attempt has been made to treat the kinetics of OH + NO and H + NO_2 reactions by considering all the competitive channels in the HNO_2 PES. It is interesting to note that the reaction of the hydroxyl anion with nitric oxide (OH^- + NO) has recently been examined both experimentally and theoretically [19]. In view of the lack of information, we set out to perform a theoretical characterisation of the reactions NO + OH and H + NO_2, which is one of the reverse reactions of the former, by making use of ab initio quantum chemical calculations followed by a detailed kinetic analysis using QRRK theory. Using this combined approach, we have recently analysed a number of bimolecular reactions involving either the NO or OH radical, namely CH_3 + NO [20], SiH_3 + NO [21], HCCO + NO [22] and OH + HNCO [23]. It is needless to say that even though the QRRK formalism is less rigorous than the RRKM, the overall reaction mechanism can be extracted from this simple treatment. Concerning the values of rate constants, both treatments give overall comparable values as they are mainly determined by geometrical and energetic parameters. The main advantage of the QRRK treatment lies in the fact that it is easy to implement it for chemically activated reactions containing several energised intermediates and multiple channels.

2. Computational methods

Ab initio molecular orbital (MO) and density functional theory (DFT) calculations were carried out using Gaussian 94 [24]. The stationary points on the HNO_2 potential energy surface, in their electronically lowest singlet state, were initially located and characterised by vibrational analysis using DFT with the hybrid functionals B3LYP [25] in conjunction with the 6-31G(d,p) basis set. Geometries of the relevant points were then reoptimised at the coupled cluster level of theory (CCSD(T)) [26] with the same atomic basis. QCISD(T) energy calculations have also been performed with B3LYP/6-31G(d,p) optimised geometries for barrierless pathways for which a canonical variational transition state theory (CVTST) has been applied. Relative energies between stationary points were estimated from single point electronic energy calculations by using both B3LYP and CCSD(T) methods and the larger 6-311 + + G(3df,2p) basis set on the corresponding optimised geometries. For open shell species, the unrestricted Hartree Fock (UHF) formalism has been employed.

Concerning the kinetic treatment, the QRRK method has been outlined in many previous papers [20–23,27]. The main features of both QRRK and CVTST treatments will be given while discussing the corresponding results. Throughout this paper, bond lengths are given in angstroms, bond angles in degrees, total energies in hartree, zero point vibrational energies and relative energies in kcal/mol, unless otherwise stated.

3. Quantum chemical calculations

In this paper, we consider the possible decomposition channels, 1,2- and 1,3-hydrogen shifts from the lowest singlet electronic surface of the adduct/intermediate HONO formed from OH and NO radicals. The PES related to [HNO_2] is shown in Fig. 1. The B3LYP/6-311 + + G(d,p) optimised geometries of the isomers (**1**) to (**4**) and the optimised structures of the transition states TS**1**/**2**, TS**2**/**3** and TS**3**/**4** are shown in Fig. 2. The numbers in parentheses refer to the results obtained at the CCSD(T)/6-31G(d,p) level of calculation.

The heats of reaction and activation energies with the appropriate ZPE corrections are tabulated in Table 1 along with the accepted heats of reaction at 0 K from the literature [28]. Table 2 lists the harmonic vibrational frequencies (unscaled) of the isomers (**1**) to (**4**) and of the various saddle points. Also the

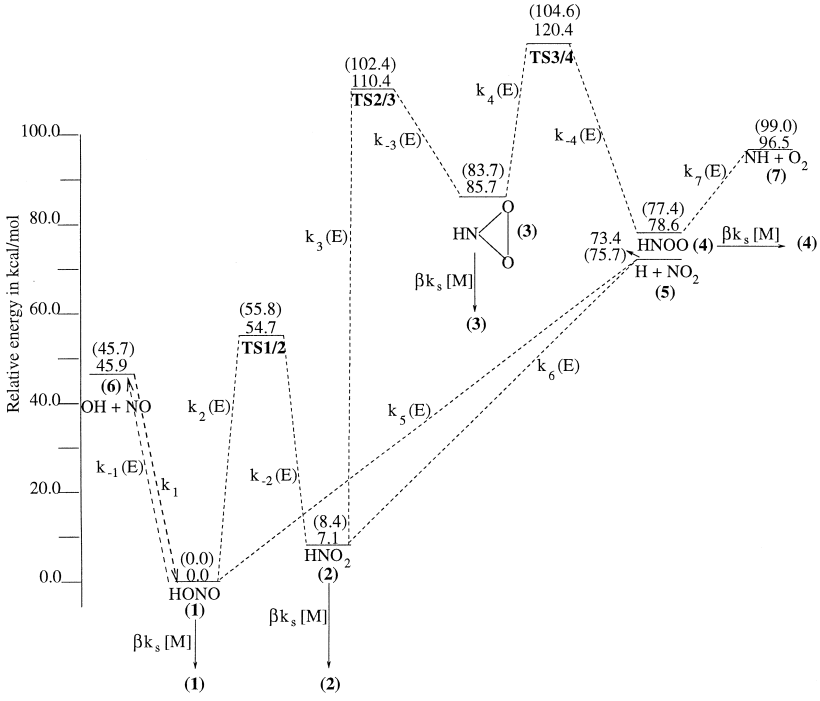

Fig. 1. The overall profile of potential energy surface for the [HNO_2] system calculated at CCSD(T)/6-311 + + G(3df,2p)//CCSD(T)/6-31G(d,p) and B3LYP/6-311 + + G (3df,2p)//B3LYP/6-311 + + G(d,p) levels of theory with ZPE corrections. Numbers in parentheses refer to the energies obtained at the former level of calculation.

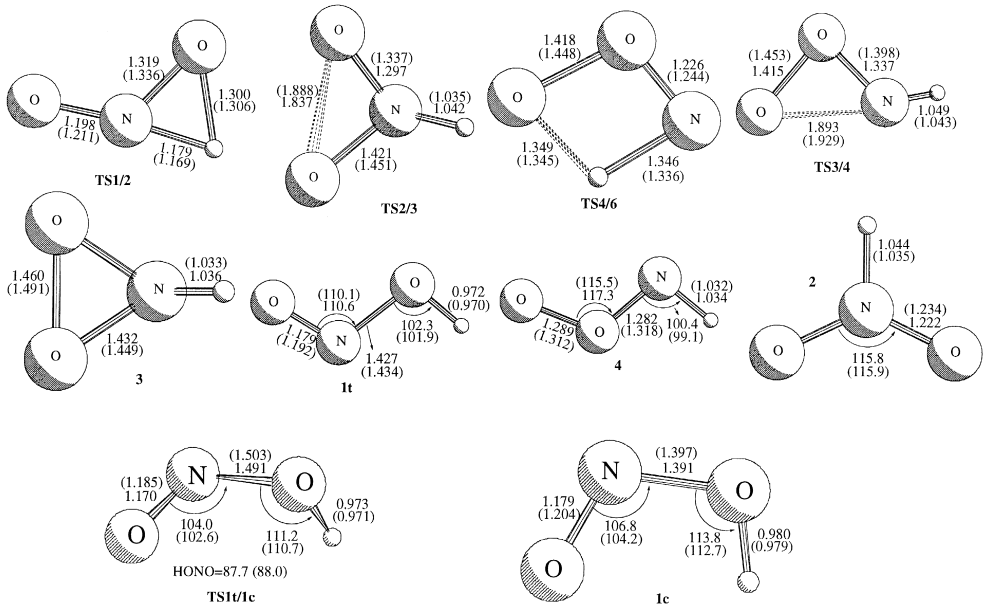

Fig. 2. B3LYP/6-311 + + G(d,p) optimised geometries (in Å and deg) of the equilibrium structures of HONO (**1**), HNO_2 (**2**), cyclic HNO_2 (**3**), HNOO (**4**) along with the transition structures TS**1**/**2**, TS**2**/**3**, TS**3**/**4** and TS**4**/**6** in [HNO_2] system. Numbers in parentheses refer to the CCSD(T)/6-31G(d,p) level of optimisation.

Table 1
Calculated heats of reaction and energy barriers at B3LYP/6-311++G(3df,2p)//B3LYP/6-31G** and CCSD(T)/6-311++G(3df,2p)//CCSD(T)/6-31G** levels in kcal/mol with ZPE corrections

Reaction	Heats of reaction			Energy barriers	
	B3LYP	CCSD(T)	Expt.	B3LYP	CCSD(T)
OH + NO (**6**) → HONO (**1**)	−45.9	−45.7	−49.2	0.0	0.0
H + NO_2 (**5**) → HNO_2 (**2**)	−66.3	−67.3		0.0	0.0
H + NO_2 (**5**) → HONO (**1**)	−73.4	−75.7	−78.3	0.0	0.0
HONO (**1**) → HNO_2 (**2**)	7.1	8.4		54.7	55.8
HNO_2 (**2**) → c-HNO_2^* (**3**)	78.6	75.3		103.3	94.0
c-HNO_2^* (**3**) → HNOO (**4**)	−7.2	−6.3		34.6	20.9
HNOO (**4**) → HN + O_2 (**7**)	17.9	21.6		17.9	21.6

* corresponds to cyclic structure.

experimental frequencies [28] of trans-HONO are also tabulated within brackets.

The OH radical can attack at the nitrogen as well as the oxygen end of the NO radical and thereby giving rise to HONO and NOOH adducts, respectively. However, the attack of the OH radical at the oxygen end of NO yields the highly unstable NOOH singlet nitrene. Hence, the primary step of the reaction between hydroxyl radical and nitric oxide is assumed to be the association reaction giving rise to the energised singlet adduct, HONO (**1**) with an excess energy of ~46 kcal/mol above its zero point vibrational level. Nitrous acid can exist in both cis and trans forms and the trans form is relatively more stable (0.35 kcal/mol) compared to the cis. Experimentally [28] estimated energy difference between the cis- and trans-forms of HONO is 0.50 ± .25 kcal/mol. The barrier height to cis-trans isomerisation of HONO was calculated to be 9.83 kcal/mol, a value much below the available energy of HONO. Since the trans isomer is the more stable form, we perform the rest of the calculations starting from the trans isomer. Energised HONO, in turn, can either undergo a 1,2- hydrogen shift leading to HNO_2 (**2**) or dissociate to atomic hydrogen and NO_2. The 1,2-hydrogen shift was found to proceed via the transition state TS**1**/**2** and faces an energy barrier of 55.8 kcal/mol. TS**1**/**2** lies energetically above the reactants and hence the reaction can be competitive with redissociation and/or stabilisation of the HONO adduct only at high temperatures. The dissociation of HONO into H + NO_2 (**5**) is a direct destabilisation step requiring an energy of 75.7 kcal/mol.

The possible channels from HNO_2 (**2**) comprise H–N bond cleavage leading to H and NO_2 radicals and the cyclisation of the NO_2 fragment giving rise

Table 2
Unscaled B3LYP/6-31G(d,p) harmonic vibrational frequencies of the minima and saddle points in HNO_2 PES. Zero point energies are given in kcal/mol. The values inside the parentheses refer to experimental frequencies

HONO **1**c	HONO **1**t	HNO_2 **2**	HNO_2^* **3**	HNOO **4**	TS**1**/**2**	TS**2**/**3**	TS**3**/**4**	TS**4**/**6**	TS**1**t/**1**c
647.8 (525)	595.7 (544)	783.0	797.2	678.1	**2**076.4i	**1**431.7i	**9**95.9i	**1**974.1i	**6**84.3i
736(638)	630.9 (598)	1052.1	849.5	829.9	473.8	895.4	817.8	813.6	578.7
921 (855)	861.8 (794)	1415.6	1200.2	1144.4	684.5	1075.4	945.4	938.3	810.5
1349 (1330)	1306.3 (1260)	1521.8	1227.9	1274.9	1298.9	1236.7	1220.3	1216.9	1078.7
1726 (1639)	1792.5 (1696)	1704.3	1439.8	1575.2	1633.4	1346.1	1469.9	1469.0	1799.5
3575 (3462)	3754.4 (3590)	3163.7	3287.0	3341.9	2506.3	3155.3	3140.7	2093.3	3746.1
12.8	12.8	13.8	12.6	12.6	9.43	11.02	10.9	9.34	11.5

* corresponds to cyclic structure.

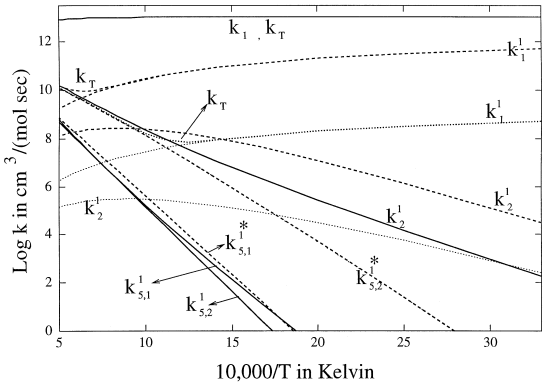

Fig. 3. Plots of log apparent rate constants of OH + NO system versus $10^{-4}/T$ (K) at 0.001 atm, 1 atm, and at high pressure limits. Dotted lines represent 0.001 atm, dashed lines represent 1 atm and the solid lines represent the high pressure.

to the energetically unfavourable cyclic HNO_2 (**3**). The PES as a function of ONO angle has been traced and the position of the transition state (TS**2**/**3**) for this reaction has been located. The reaction is highly endothermic at both CCSD(T) and B3LYP levels. The barrier for cyclisation (95.9 kcal/mol) is much higher than that for bond dissociation (67.3 kcal/mol). Moreover, the dissociation limit, H + NO_2 (**5**), lies above the reactant radicals (OH + NO) thereby suggesting stabilisation of the HNO_2 (**2**) isomer as a more likely product route.

The cleavage of an N–O bond in cyclic HNO_2 (**3**) can give rise to the relatively stable HNOO (**4**) biradical (Fig. 1) via the transition state, TS**3**/**4** (Fig. 3). The HNOO biradical can then undergo 1,3-hydrogen migration leading to the unstable singlet NOOH nitrene. The possible transition state for 1,3-hydrogen migration (TS**4**/**5**) has been located and is shown in Fig. 2. The 1,3-hydrogen migration in HNOO is accompanied by the simultaneous elongation of the O–O bond and it leads to NO and OH. All our attempts to obtain the minimum energy structure of the singlet NOOH nitrene are proved futile. The remarkably high barrier for the conversion of (**2**) to (**3**) prevents the possible involvement of cyclic HNO_2 (**3**) and HNOO (**4**) species in the kinetics of OH + NO (**6**) reaction. However, they have been included in our detailed kinetic analysis.

4. Kinetic analyses

In the present section, we calculate the apparent rate constants of (1) OH + NO, (2) H + NO_2 (via HONO) and (3) H + NO_2 (via HNO_2) using QRRK theory. Various product channels of these reactions are shown in Fig. 1. The reactions in Fig. 1 involve a competition between stabilisation and dissociation of the energised adducts and should not be treated as elementary single-step reactions. Such reactions involving the formation of highly energized adducts should rather be treated using the idea of chemical activation [29]. We use the potential energy surface obtained at the CCSD(T)/6-311 + + G(3df,2p)//CCSD(T)/6-31G(d,p) level and the vibrational frequencies and rotational constants calculated at the B3LYP/6-31G(d,p) level as input parameters for the QRRK calculations. Recent publications [20–23,30] reveal that processes involving high energy chemically activated adducts with non-Boltzmann distribution can be accurately characterized by the QRRK method.

4.1. QRRK analysis of the OH + NO reaction (reaction 1)

The apparent rate constants of various channels for the OH + NO reaction are defined as

k_1^1:	OH + NO	→	HONO (**1**)
$k_{5,1}^1$:	OH + NO	→	H + NO_2 (**5**) (via HONO (**1**))
k_2^1:	OH + NO	→	HNO_2 (**2**)
$k_{5,2}^1$:	OH + NO	→	H + NO_2 (**5**) (via HONO (**1**) and HNO_2 (**2**))
k_3^1:	OH + NO	→	HNO_2 (Cyclic) (**3**)
k_4^1:	OH + NO	→	HNOO (**4**)
k_7^1:	OH + NO	→	NH + O_2 (**7**) (via HNOO (**4**))

The apparent rate constant for stabilisation of, say (**1**), can be calculated as

$$k_1^1 = \beta k_s[\mathrm{M}] \sum_{E_{\mathrm{crit}}}^{\infty} [1*] f(E)/[\mathrm{OH}][\mathrm{NO}].$$

Similarly, the apparent rate constant for a dissociation pathway, for example, $k^1_{5,2}$, can be written as

$$k^1_{5,2} = \sum_{E^{\infty}_{crit}} k_5(E)[3*]f(E)/[OH][NO],$$

where $[1*]$ and $[3*]$ are the steady state concentrations of (**1**) and (**3**), respectively. Similar expressions were followed to calculate other apparent rate constants for the reactions H + NO_2 → HONO and H + NO_2 → HNO_2. The expression for $f(E)$, the chemical activation distribution function is taken from Ref. [29]. M is the bath gas (N_2 for the present study) and $k_i(E)$'s are the energy dependent unimolecular rate constants which are calculated using the QRRK theory. The steady state concentrations of the energised adduct and the isomers can readily be expressed in terms of the $k_i(E)$'s. The method of calculation of the energy dependent rate constant has been discussed elsewhere in detail [14,27]. In essence, quantum Kassel theory uses statistical mechanics to calculate the probability that sufficient energy will be localised in a given oscillator for reaction to occur. Though, RRKM, the improved technique, is more accurate in principle, it calculates the *A*-factor for dissociation from the assumed properties of the transition state and the reactant, i.e., the vibrational and internal rotor frequencies, the state densities and rotational parameters. As a consequence, the uncertainties in the input parameters may restrict its predictive value, unless significant effort is put into the assignment. While we encourage the use of the more rigorous RRKM treatments where appropriate, this option is more tedious in the present case which involves four dissociation channels. Dean et al. in their QRRK analysis [14,27], either use the experimentally measured value for the Arrhenius *A*-factors or estimate the same based on isoelectronic or structurally similar reactants with known kinetic parameters. It, thus, provides a room for the adjustment of the input parameters. We use the averaged Arrhenius parameters within the transition state theory framework in our calculation. Though, it is less appropriate, it provides a simpler way to treat the kinetics of the multichannel system without adjusting any of the input parameters. From our experience [20,21,23,30], we could explain the total magnitude as well as the *T* and *P* variation of the rate coefficient to a reasonably good extent by using this approach.

The frequency factors for isomerisation of chemically activated species and for the unimolecular reactions with specific transition states were calculated as

$$A_i = \frac{k_B T}{h}\frac{Q^{\dagger}_i}{Q_i},$$

where k_B is the Boltzmann constant, h the Planck's constant, T the temperature in Kelvin and $Q^{\dagger}_i$ and Q_i are the complete partition functions for the respective transition state and the reactant, respectively. The partition functions were obtained from our ab initio calculated harmonic vibrational frequencies and moments of inertia at the B3LYP/6-31G(d,p) level.

The frequency factors for the barrierless recombination and dissociation reactions were obtained via canonical variational transition state theory (CVTST) [31]. According to the CVTST, the rate constant at temperature T is obtained by maximising $\Delta G^0(T,s)$ with respect to s, the reaction coordinate. The rate constant k for temperature T evaluated at the dividing surface s can be written as

$$k(T,s) = \frac{k_B T}{h}\exp\left(-\Delta G^0(T,s)/k_B T\right).$$

Here, k_B is the Boltzmann constant; h is the Planck's constant; s is the reaction coordinate, and $\Delta G^0(T,s)$ is the standard-state free energy of activation on the dividing surface at s. In order to find the maximum ΔG^0 for each temperature, we first calculated the complete potential energy surfaces for the approach of HO to NO (reaction 1) and of H to oxygen (reaction 2) and to nitrogen (reaction 3) atoms of NO_2. The forming bond distance in every case was varied from 1.5 Å to 2.8 Å with an increment of 0.1 Å. For each value of the forming bond distance, other geometric parameters were completely optimised at B3LYP level. For each structure, we calculated the $3N-7$ vibrational frequencies, projected out of the gradient direction. We then performed a QCISD(T) calculation for each optimised geometry in order to obtain the more reliable energies. Furthermore, we used a Morse potential to fit the potential energy calculated at the QCISD(T) level. The fitted β values for OH + NO, H + ONO and H + NO_2 potential energy surfaces are 3.372, 5.444 and 3.30 $Å^{-1}$, respectively. The fitting of the PES has been

done, in order to obtain an analytical function which can be maximised. Similar procedure was used by Hsu et al. [32] to obtain the rate constant for the barrierless combination of HCO to O_2. The Morse potential energy, computed moments of inertia and vibrational frequencies were used for the calculation of ΔG^0. We looked for the maximum $\Delta G^0(T,s^\dagger)$ at various temperatures in the range of 300 to 2000 K. $s^\dagger$ corresponds to the reaction coordinate at maximum ΔG^0. Using the maximum $\Delta G^0(T,S^\dagger)$'s, we calculated the rate constants as a function of temperature and these values are then fitted with the Arrhenius equation,

$$k = A\exp(-E_a/RT)$$

to obtain the best fit value of A, the frequency factor and E_a, the activation barrier. The frequency factors thus calculated for various reactions being,

$OH + NO \rightarrow HONO$,
$A = 1.04 \times 10^{13}\ cm^3\ mol^{-1}\ s^{-1}$
$HONO \rightarrow OH + NO$,
$A = 6.13 \times 10^{14}\ s^{-1}$
$H + ONO \rightarrow HONO$,
$A = 2.45 \times 10^{13}\ cm^3\ mol^{-1}\ s^{-1}$
$HONO \rightarrow H + ONO$,
$A = 6.69 \times 10^{13}\ s^{-1}$
$H + NO_2 \rightarrow HNO_2$,
$A = 3.95 \times 10^{13}\ cm^3\ mol^{-1}\ s^{-1}$
$HNO_2 \rightarrow H + NO_2$,
$A = 2.40 \times 10^{14}\ s^{-1}$

We then use these fitted A's in our QRRK program to obtain the unimolecular dissociation rate constants. The bimolecular rate constant, k_1 for the combination of OH and NO was calculated by using the Arrhenius rate expression with the fitted frequency factor and activation barrier. For the description of the collisional stabilisation, we adopted the weak collision model suggested by Troe [33,34] and the collision rate is considered to be a product of the Lennard-Jones collision frequency, Z_{LJ} and collision efficiency, β. The collision efficiency, β, was calculated from [34]

$$\frac{\beta}{1-\beta^{\frac{1}{2}}} = -\langle\Delta E\rangle/F_E k_B T.$$

Though it is more appropriate to use the chemical activation collision efficiency, γ, of Troe [35], we continue to use β for the sake of simplicity. However, the use of β will not affect the total magnitude of k. The value of F_E was assumed to be 1.15 and the $\langle\Delta E\rangle$, average energy transferred per collision, was taken as 1.6 kJ/mol for N_2 as bath gas following the reference of Hippler et al. [36]. The entire QRRK calculation was performed using the program KWANT-RATE [37] developed in our group.

The calculated apparent rate constants, k_3^1, k_4^1 and k_7^1 were found to be very low and therefore are of little importance and hence will not be discussed any further. The total rate constant, k_T for the disappearance of the reactants was calculated as sum of all apparent rate constants. Fig. 3 shows the variation of the apparent rate constants for the formation of the adduct and various products with temperature. The solid lines correspond to a high pressure (10^5 atm) while the dashed and dotted lines correspond respectively to a pressure of 1 and 0.001 atm. At all pressures, the $H + NO_2$ channel opens up only at higher temperatures. This is due to the fact that at lower temperatures the number of HONO molecules formed with energy greater than or equal to the energy of $H + NO_2$ is small. Consequently, at lower temperatures, stabilisation of the adduct becomes the primary channel for the disappearance of the reactants. At low pressures, most of the initially activated HONO formed will redissociate to OH + NO. Increasing the pressure to a very high value results in stabilisation of almost all the HONO. To open up the dissociation channels at very high pressure, a very high temperature is necessary. The value of k_T obtained from our calculation at 297 K and 1 atm is $5.08 \times 10^{11}\ cm^3\ mol^{-1}\ s^{-1}$ while the recent reported value [38] is $4.45 \times 10^{12}\ cm^3\ mol^{-1}\ s^{-1}$.

Fig. 4 shows the variation of the apparent rate constants as a function of the total pressure at 300 K. It shows that at 300 K, HONO formation is the dominant channel at all pressures. The total rate constant and hence k_1^1 becomes pressure independent at a pressure of 10^3 atm. This observation is consistent with the experimental results of Bohn et al. [38], wherein they observe an increase in the rate constant with increasing pressures until 1 atm. However, our calculated values are a factor of 8 lower than the experimental value. Nevertheless, our calculated k_∞

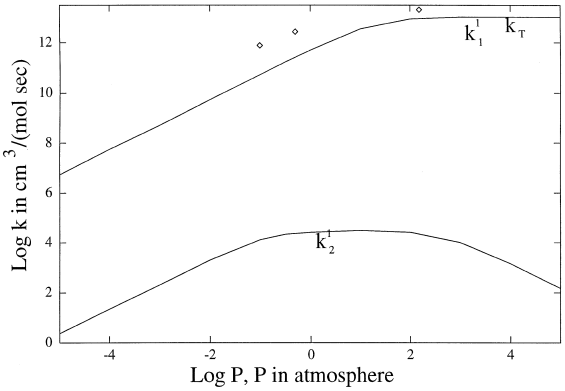

Fig. 4. Plots of log apparent rate constants and total rate constant of OH + NO reaction versus log pressure at 298 K. ◇ corresponds to experimental values from Refs. [16,38].

value at 300 K (1.04×10^{13} cm^3 mol^{-1} s^{-1}) is in very good agreement with the earlier reported value [16] of 1.9×10^{13} cm^3 mol^{-1} s^{-1} by Hippler and Troe. Pagsberg et al. [39] have recently reported the limiting low pressure rate constant $k_0/[SF_6]$ to be $5.4 \pm 0.1 \times 10^{17}$ cm^6 mol^{-2} s^{-1} at 298 K and they have used the k_∞ value of Hippler and Troe [16]. Our calculated k_0 (1.65×10^{16} cm^6 mol^{-2} s^{-1}) is an order of magnitude lower than the experimental value. The experimental ratio of k_0/k_∞ equals 2.8×10^4 while the calculated ratio being 1.6×10^3. This could mean that back dissociation to OH and NO has been slightly overestimated in our treatments.

4.2. QRRK analysis of H + NO_2 reaction (reaction 2 and 3)

The H + NO_2 reaction can give rise to either HONO (**1**) or HNO_2 (**2**) as the initially formed energised adduct and hence the kinetics of this reaction has been analysed by starting from both HONO (Reaction 2) and HNO_2 (Reaction 3) potential wells. The several product channels which are energetically possible include OH + NO (**6**), HONO(**1**), HNO_2 (**2**) as well as the reformation of H + NO_2 (**5**) via HNO_2 and HONO. We use the same PES obtained for the OH + NO reaction for our kinetic analysis.

The competitive reactions starting from H + NO_2 are also shown in Fig. 1. Two possible adducts can be formed depending on whether the H atom adds to O or N centers of NO_2 radical. Since the rate constants for product formation depend highly on the internal energy of the adduct, the product distributions originating from these two additions are expected to be markedly different. A glance at the PES (Fig. 1) reveals that when the more stable HONO is formed initially, it undergoes at low pressures a preferential dissociation to OH + NO radicals due to its low barrier height and to the larger magnitude of the frequency factor for a dissociation reaction.

For the reaction 2, we define the apparent rate constants for the various pathways in Fig. 1 as follows

k_1^2: H + NO_2 → HONO (**1**)
k_2^2: H + NO_2 → HNO_2 (**2**) (via HONO (**1**))
k_6^2: H + NO_2 → HO + NO (**6**)
k_5^2: H + NO_2 → H + NO_2 (**5**) (via HNO_2 (**2**))
k_3^2: H + NO_2 → HNO_2 (Cyclic) (**3**)
k_4^2: H + NO_2 → HNOO (**4**)
k_7^2: H + NO_2 → HN + O_2 (**7**)

Similarly, for the reaction 3,

k_1^3: H + NO_2 → HONO (**1**) (via HNO_2 (**2**))
k_2^3: H + NO_2 → HNO_2 (**2**)
k_5^3: H + NO_2 → H + NO_2 (**5**) (via HNO_2 (**2**) and HONO (**1**))
k_6^3: H + NO_2 → HO + NO (**6**) (via HNO_2 (**2**) and HONO (**1**))
k_3^3: H + NO_2 → HNO_2 (Cyclic) (**3**)
k_4^3: H + NO_2 → HNOO (**4**)
k_7^3: H + NO_2 → HN + O_2 (**7**)

The superscript and subscript in the rate constant definition correspond, respectively, to the reaction number and the product number as shown in Fig. 1. Apparent rate constants of these two reactions are calculated following a similar procedure to that for reaction 1. The apparent rate constants, k_3^2, k_3^3, k_4^2, k_4^3, k_7^2 and k_7^3 are very low due to their higher activation barrier for their formation. These pathways, therefore, have little importance in the destruction of the reactants. The total rate constant for the disappearance of the reactants was calculated as the sum of all apparent rate constants except k_5^2 and k_5^3, since these channels regenerate the reactants H + NO_2(**5**).

Fig. 5 shows the variation of the apparent rate constants as a function of pressure at 300 K. The predominant contributions to the total rate constant come from k_6^2 and k_6^3 except at very high pressures

where the stabilisation of HONO (**1**) and HNO_2 (**2**) outruns their dissociation to OH + NO (**6**). In the lower pressure region, both k_1^2 and k_2^2 increase with increasing pressure. In the high pressure region, while k_1^2 reaches a limiting value, k_2^2 decreases after passing through a maximum. This is due to the fact that at lower pressures (**1**) → (**2**) isomerisation is appreciable even though the main channel is (**1**) → OH + NO (**6**) (k_6^2). At very high pressures, stabilisation of (**1**) takes place at the cost of (**1**) → (**2**) isomerisation, thereby reducing k_2^2. Similarly, for reaction 3, k_2^3 increases with increasing pressure while k_6^3 decreases. This is due to the faster stabilisation of (**2**) that prevents (**2**) → (**1**) isomerisation, thereby reducing HO + NO formation. Fig. 6 displays the variations of all the apparent rate constants for reactions (2) and (3) with temperature at atmospheric pressure. At all temperatures, formation of OH + NO (**6**) is found to be the predominant channel. Rate constant for OH + NO formation in reactions (2) and (3) are nearly the same below 1 atmosphere pressure. However, at pressures higher than 10 atmosphere OH + NO formation occurs predominantly via reaction (2).

4.3. Some thermochemical data

The heats of formation of HONO and HNO_2 have been calculated by using the exchange reaction, HNO + H_2O → HNO_2 + H_2. The heat of formation of HNO was taken as 26.0 kcal/mol following the reference of Lee [40] and the heat of formation of water was taken from the tables [41]. The calculated heats of formation at the B3LYP level for HONO and HNO_2 being −19.1 and −13.9 kcal/mol respectively. While at the CCSD(T) level, they correspond respectively to −16.7 and −10.3 kcal/mol. The proton affinity of the NO_2 radical at both the oxygen and nitrogen sites have been computed as the negative of the enthalpy change associated with the reaction, $NO_2 + H^+ \rightarrow HONO^+$ (or) HNO_2^+. The values obtained suggest a higher probability of protonation at oxygen site (at 298 K, 139.5 and 140.5 kcal/mol at B3LYP and CCSD(T) levels, respectively) compared to the nitrogen end (104.6 and 86.6 kcal/mol at B3LYP and CCSD(T) levels, respectively). It is important to mention that the experimental proton affinity of NO_2 species is 140 kcal/mol and that our calculated values are in good agreement with the experimental values. The ionisation energies of HONO and HNO_2 were found respectively to be 10.9 and 12.1 eV and are taken as the energy difference of the corresponding positively charged ion and the neutral molecule. Using the proton affinity value and the ionisation energy, we have found that the heats of formation of HONO and HNO_2 at CCSD(T) level are −16.8 and −6.5 kcal/mol, respectively. Though the ΔH_f value for HONO is very close as calculated by two methods, the corresponding value for HNO_2 shows an appreciable change and we attribute it to the difficulty in treating the symmetry broken structure of HNO_2^+. We suggest that the heat of formation of HONO can be taken as $\Delta H^0_{f,298}$(HONO) = −16.8 kcal/mol and

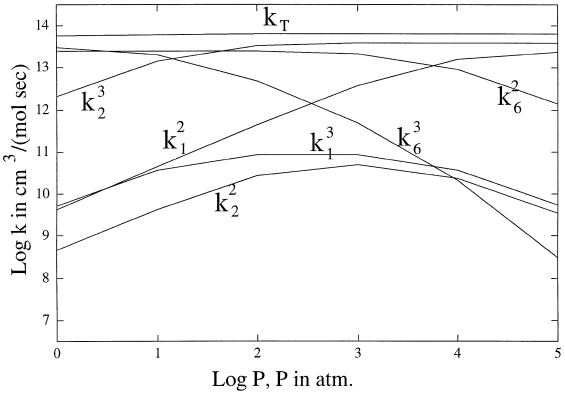

Fig. 5. Plots of log apparent rate constants and total rate constant of H + NO_2 reaction versus log pressure at 298 K.

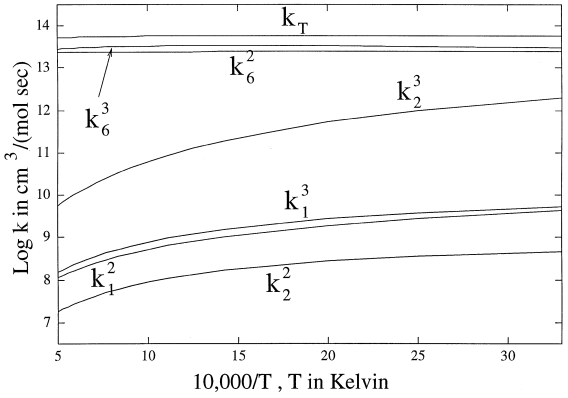

Fig. 6. Plots of log apparent rate constants of H + NO_2 system versus $10^4/T$ (K) at 1 atmospheric pressure.

$\Delta H^0_{f,298}(HNO_2) = -8.5$ kcal/mol, with a probable error of ± 2 kcal/mol.

5. Conclusion

Potential energy surface of $[HNO_2]$ isomers and related dissociation pathways have been explored by means of ab initio molecular orbital calculations at CCSD(T) level and DFT methods using B3LYP as functionals. The results of the quantum chemical calculations were further utilised to calculate the rate constants of (1) OH + NO, (2) H + NO_2 (via HONO) and (3) H + NO_2 (via HNO_2) reactions using a bimolecular version of QRRK theory. Our calculated results show that, for reaction 1, while HONO formation is the predominant channel at lower temperatures, at higher temperatures H + NO_2 formation can also become important. OH + NO formation in the reaction H + NO_2 occurs by the addition of hydrogen on an oxygen of the NO_2 radical (reaction 2) as well as on the nitrogen (reaction 3) below 1 atmosphere pressure. Some thermochemical data such as the heats of formation of HONO and HNO_2 and the proton affinity of NO_2 radical have been reported at the highest level of our calculation.

Acknowledgements

We are indebted to the Fund for Scientific Research (FWO-Vlaanderen) and Geconcerteerde Onderzoeksakties (GOA) for financial support and to the KU Leuven Computer Center for providing computer facilities.

References

[1] C. Zetzsch, I. Hansen, Ber. Bunsenges. Phys. Chem. 82 (1978) 830.
[2] J.H. Bromly, F.J. Barnes, P.F. Nelson, B.S. Haynes, Int. J. Chem. Kinet. 27 (1995) 1165.
[3] W. Hack, H. Kurzke, H.Gg. Wagner, J. Chem. Soc. Faraday Trans. II 81 (1985) 949.
[4] M.A.A. Clyne, B.A. Thrush, Trans. Faraday Soc. 57 (1961) 2176.
[5] A. Mckenzie, M.F.R. Mulcahy, J.R. Steven, J. Chem. Soc. Faraday Trans. I 70 (1974) 549.
[6] J.E. Spencer, G.P. Glass, Chem. Phys. 15 (1976) 35.
[7] H.Gg. Wagner, U. Welzbacher, R. Zellner, Ber. Bunsenges. Phys. Chem. 80 (1976) 1023.
[8] W.A. Guillory, C.E. Hunter, J. Chem. Phys. 54 (1971) 598.
[9] R. Forster, M. Frost, D. Fulle, H.F. Hamann, H. Hippler, A. Schlepegrell, J. Troe, J. Chem. Phys. 103 (1995) 2949.
[10] J.A. Miller, M.D. Smooke, R.M. Green, R.J. Kee, Combust. Sci. Technol. 34 (1983) 149.
[11] A.M. Dean, M.S. Chou, D. Stern, Int. J. Chem. Kinet. 16 (1984) 633.
[12] W. Tsang, J. Phys. Chem. Ref. Data 20 (1991) 221.
[13] O.M. Vandooren, O.M. Sarkisov, V.P. Balakhnin, P.J. Van Tiggelen, Chem. Phys. Lett. 184 (1991) 294.
[14] A.M. Dean, J.W. Bozzelli, Combustion Chemistry II, in: W.C. Gardiner Jr. (Ed.), Springer, to be published.
[15] R. Cotting, J.R. Hubert, J. Chem. Phys. 104 (1996) 6208, and references cited therein.
[16] R. Atkinson, D.L. Baulch, R.A. Cos, R.F. Hampson Jr., J.A. Kerr, J. Troe, Atm. Env. 26 A (1992) 1187; R. Forster, M. Frost, D. Fulle, H.F. Hamann, H. Hippler, A. Schlepegrell, J. Troe, J. Chem. Phys. 103 (1995) 2949.
[17] T. Fueno, K. Tokayama, S. Takane, Theoret. Chim. Acta 82 (1992) 299.
[18] S. Takane, T. Fueno, Theoret. Chim. Acta 87 (1994) 431.
[19] J.M. Vandooren, A.A. Viggiano, R.A. Morris, A.M. Stevens Miller, T.M. Miller, J.F. Paulson, C.A. Deakyne, H.H. Michels, J.A. Montgomery, J. Chem. Phys. 98 (1993) 7940.
[20] M.T. Nguyen, D. Sengupta, L.G. Vanquickenborne, J. Phys. Chem. 100 (1996) 10956.
[21] D. Sengupta, M.T. Nguyen, Chem. Phys. Lett. 265 (1997) 35.
[22] M.T. Nguyen, W. Boulart, J. Peeters, J. Phys. Chem. 98 (1994) 8030.
[23] D. Sengupta, M.T. Nguyen, J. Chem. Phys. 106 (1997) 9703.
[24] M.J. Frisch, G.W. Trucks, H.B. Schlegel, P.M.W. Gill, B.G. Johnson, M.A. Robb, J.R. Cheeseman, T. Keith, G.A. Petersson, J.A. Montgomery, K. Raghavachari, M.A. Al-Laham, V.G. Zakrzewski, J.V. Ortiz, J.B. Foresman, J. Cioslowski, B.B. Stefanov, A. Nanayakkara, M. Challacombe, C.Y. Eng, P.Y. Ayala, W. Chen, M.W. Wong, J.L. Andres, E.S. Replogle, R. Gomperts, R.L. Martin, D.J. Fox, J.S. Binkley, D.J. Defrees, J. Baker, J.P. Stewart, M. Head-Gordon, C. Gonzalez, J.A. Pople, Gaussian, Inc., Pittsburgh PA, 1995.
[25] P.J. Stephens, F.J. Devlin, C.F. Chabalowski, M.J. Frisch, J. Phys. Chem. 45 (1994) 98.
[26] G.D. Purvis, R.J. Bartlett, J. Chem. Phys. 76 (1982) 1910.
[27] A.M. Dean, J. Phys. Chem. 89 (1985) 4600.
[28] M.W. Chase Jr., C.A. Davies, J.R. Downey Jr., D.J. Frurip, R.A. McDonald, A.N. Syverud, J. Phys. Chem. Ref. Data 14 (1985) Suppl. No. 1.
[29] P.J. Robinson, K.A. Holbrook, Unimolecular Reactions, Wiley Interscience, London, 1972.
[30] R. Sumathi, S.D. Peyerimhoff, Chem. Phys. Lett. 263 (1996) 742; R. Sumathi, S.D. Peyerimhoff, J. Chem. Phys. 107 (1997) 1872; A.M. Dean, P.R. Westmoreland, Int. J. Chem. Kinet. 19 (1987) 207.
[31] B.C. Garrett, D.G. Truhlar, J. Phys. Chem. 83 (1979) 1052; B.C. Garrett, D.G. Truhlar, J. Chem. Phys. 70 (1979) 1593.

[32] C.-C. Hsu, A.M. Mebel, M.C. Lin, J. Chem. Phys. 105 (1996) 2346.
[33] J. Troe, J. Chem. Phys. 66 (1977) 4758.
[34] J. Troe, J. Chem. Phys. 83 (1979) 114.
[35] J. Troe, J. Phys. Chem. 87 (1983) 1800; D. Fuller, H.F. Hamann, H. Hippler, J. Troe, J. Chem. Phys. 105 (1996) 983.
[36] H. Hippler, J. Troe, H.J. Wendelken, J. Chem. Phys. 78 (1983) 6709.
[37] D. Sengupta, M.T. Nguyen, KWANT-RATE, A Program to calculate rate constants for multichannel chemically activated reactions via QRRK Theory, University of Leuven, 1996.
[38] B. Bohn, C. Zetzsch, J. Phys. Chem. A 101 (1997) 1488.
[39] P. Pagsberg, E. Bjergbakke, E. Ratajczak, A. Sillesen, Chem. Phys. Lett. 272 (1997) 383.
[40] T.J. Lee, J. Chem. Phys. 103 (1995) 9110.
[41] S.G. Lias, J.E. Bartmess, J.F. Liebman, J.L. Holmes, R.D. Levin, W.G. Mallard, J. Phys. Chem. Ref. Data 17 (Suppl. 1) (1988) 621.